LEGIBILITY NOTICE

A major purpose of the Technical Information Center is to provide the broadest dissemination possible of information contained in DOE's Research and Development Reports to business, indust the academic community, and feueral, state and local governments.

Although a small portion of this report is not reproducible, it is being made available to expedite the availability of information on the research discussed herein.

LA-UR-82-2504

Conf-830301--2

Los Alamos National Laboratory is operated by the University of California for the United States Department of Energy under contract W-7405-ENG-36.

TITLE: A CHAP-2 HEAT-TRANSFER ANALYSIS OF THE FORT ST. VRAIN REACTOR CORE

AUTHOR(S): Jonathan F. Kotas
Kenneth R. Stroh

SUBMITTED TO: The ASME-JSME Thermal Engineering Joint Conference
March 20-24, 1983
Honolulu, Hawaii

Los Alamos Los Alamos National Laboratory
Los Alamos, New Mexico 87545

A CHAP-2 HEAT-TRANSFER ANALYSIS OF THE FORT ST. VRAIN REACTOR CORE*

by

Jonathan F. Kotas and Kenneth R. Stroh

Safety Code Development
Energy Division
Los Alamos National Laboratory
Los Alamos, New Mexico 87545

ABSTRACT

The Los Alamos National Laboratory is developing the Composite High-Temperature Gas-Cooled Reactor Analysis Program (CHAP) to provide advanced best-estimate predictions of postulated accidents in gas-cooled reactor plants. The CHAP-2 reactor-core model uses the finite-element method to initialize a two-dimensional temperature map of the Fort St. Vrain (FSV) core and its top and bottom reflectors. The code generates a finite-element mesh, initializes noding and boundary conditions, and solves the nonlinear Laplace heat equation using temperature-dependent thermal conductivities, variable coolant-channel-convection heat-transfer coefficients, and specified internal fuel and moderator heat-generation rates. In our paper we discuss this method and analyze an FSV reactor-core accident that simulates a control-rod withdrawal at full power.

*Work performed under the auspices of the US Nuclear Regulatory Commission.

NOMENCLATURE

A	heat-transfer area
c_p	specific heat
e	unit vector
f	ratio of the length to the total height
F_{ij}	fractional contact area
h	convective heat-transfer coefficient or specific enthalpy
H	total enthalpy
K	thermal conductivity
L	channel length
P_f	normalized axial power distribution
Pr	Prandtl number
$\dot{q}$	heat-transfer rate
q'''	internal heat-generation rate
r	finite-element radial-mesh coordinate
Re	Reynolds number
t	time
T	helium-coolant temperature
U	overall composite conductivity
V	total volume
W	mass flow
x	distance along coolant channel
z	finite-element axial-mesh coordinate
∇	divergence operator
ε	emissivity
ρ	density
σ	Stefan-Boltzmann constant
ϕ	material temperature

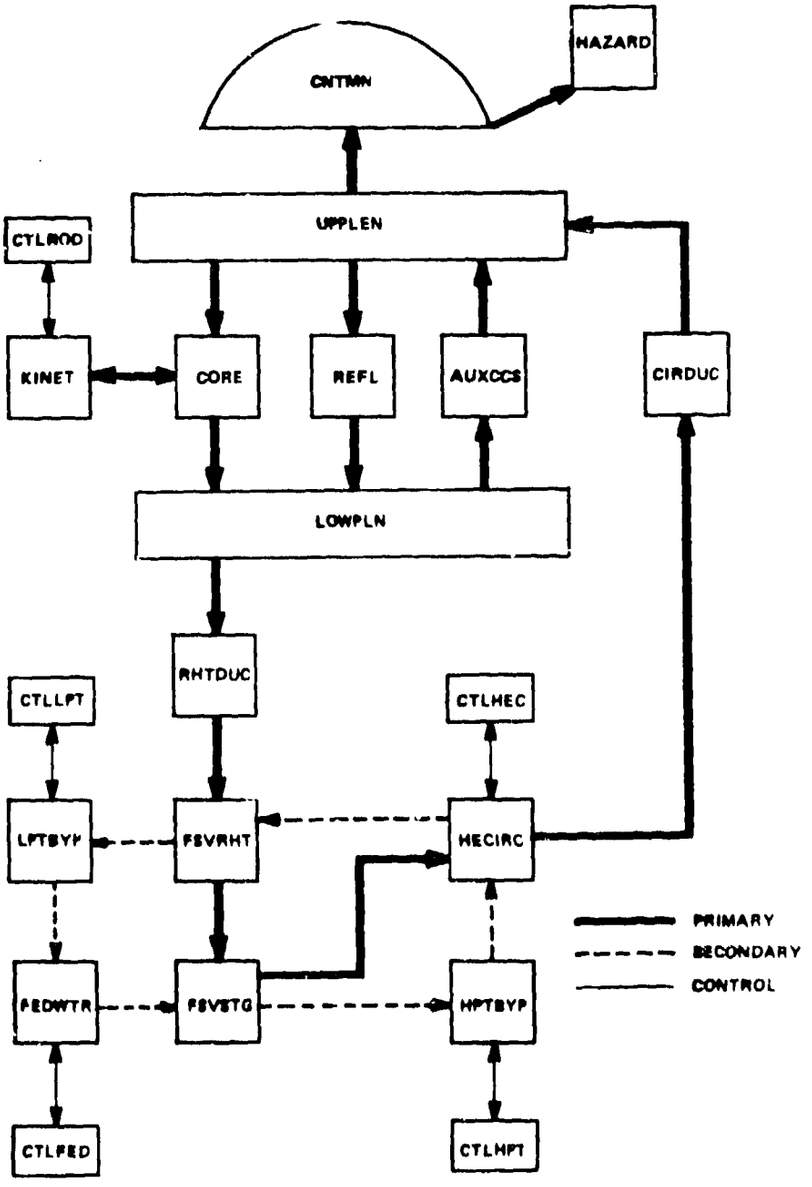

Fig. 1.
CHAP-2 modular structure.

1. INTRODUCTION

Since the beginning of the gas-cooled reactor program in the US, the General Atomic Company (GA) and the US Nuclear Regulatory Commission (NRC) extensively have used numerical methods to design and analyze such plants. General Atomic ostensibly used several computer codes to design the Fort St. Vrain (FSV) plant bought by the Public Service Company of Colorado and the 2000- and 3000-MW(t) plants bought by 10 electrical utilities in the early 1970s. These codes included BLOOST-7 (Ref. 1); RECA,[2] a general neutron-kinetics and heat-transfer program; CORCON,[3] an extensive core heat-transfer code; TAP,[4] a core heat-transfer transient analysis code; RATSAM,[5] an overall high-temperature gas-cooled reactor (HTGR) plant systems analysis code; a core heat-transfer code emphasizing the design-basis-depressurization accident (DBDA) and the loss-of-forced-circulation (LOFC) events; and RECA3,[6] an updated version of RECA. In response to the contracts between GA and the utilities, the licensing of the FSV plant, and a lack of regulatory expertise in this field, the NRC selected the Oak Ridge National Laboratory (ORNL) and the Los Alamos National Laboratory to assess independently the safety of the gas-cooled reactor plant. Consequently, Oak Ridge developed ORECA-I,[7] an extensive FSV reactor-core heat-transfer analysis code; CORTAP,[8] a coupled neutron-kinetics heat-transfer HTGR reactor-core analysis code; and ORTAP,[9] an overall plant systems analysis code. Los Alamos initially analyzed the 2000- and 3000-MW(t) plants and released CHAP-1 (Ref. 10) in March 1977. Because GA canceled its contracts on the large plants in 1975, the NRC directed Los Alamos to develop an FSV version of CHAP. The result of this continuing program is the current version of the code CHAP-2 (Ref. 11).

2. CHAP-2 DESCRIPTION

The CHAP-2 code is a best-estimate dynamic systems code describing the thermal, fluid, neutronic, and control response of an HTGR power plant. This code is designed to examine the total plant response to anticipated plant transients and postulated accidents delineated by the NRC. Thus, CHAP-2 is similar to the GA code TAP and the ORNL code ORTAP. The current version models, with equal degrees of sophistication, the FSV plant; the 3000-MW(t) plant; and GA's contemporary design, the 2240-MW(t) lead plant. The code models both the primary (gas) and the secondary (steam/feedwater) sides of the power plant. As shown in Fig. 1, the code is divided into 22 sections or modules, with each one modeling a specific plant system. Appendix A provides a

summary of the CHAP-2 modules and their definitions. The HTGR basic physical processes for a particular component or system are defined in each module and are described mathematically by a set of nonlinear simultaneous, first-order, ordinary differential equations. The code uses the state-variable approach to modeling, with each equation of the form,

$$\dot{x}_i(t) = f_i\,(x_1, \ldots, x_i, \ldots, x_n, u_1, \ldots, u_k, \ldots, u_m) \quad , \tag{1}$$

where x_i is the set of n integration or state variables; u_k, the set of m inputs to the system; and f_i, the nonlinear function describing the state x_i. The Los Alamos code LASAN[12] computes the steady-state, frequency, and time (transient) response of the system of equations defined by Eq. (1).

Postulated accidents and expected plant transients modeled by CHAP-2 include:

(1) control-rod withdrawal at full or partial power,
(2) total or partial loss of helium primary-coolant flow,
(3) total or partial loss of feedwater flow,
(4) loss of one or more steam-generator loops,
(5) loss of load or turbine trip,
(6) main or reheat steam-line break,
(7) helium circulator trip,
(8) reactor trip, and
(9) depressurization of the reactor vessel from the upper or lower plenum or both.

Although CHAP-2 can examine the total plant response of the FSV plant, the 3000-MW(t) plant, or the 2240-MW(t) lead plant to any of the above transients, we will discuss only the FSV thermal-hydraulic core model and will analyze a control-rod withdrawal accident at full power. References 11 and 12, respectively, provide further information on the CHAP-2 and LASAN codes.

3. DESCRIPTION OF THE FSV REACTOR CORE

A detailed description of the FSV plant and reactor is given in the FSV final safety analysis report (FSAR)[13] and will be discussed briefly in this section. The FSV active reactor core (Fig. 2) has the approximate shape of a right-circular cylinder. It is surrounded by top, bottom, and side graphite

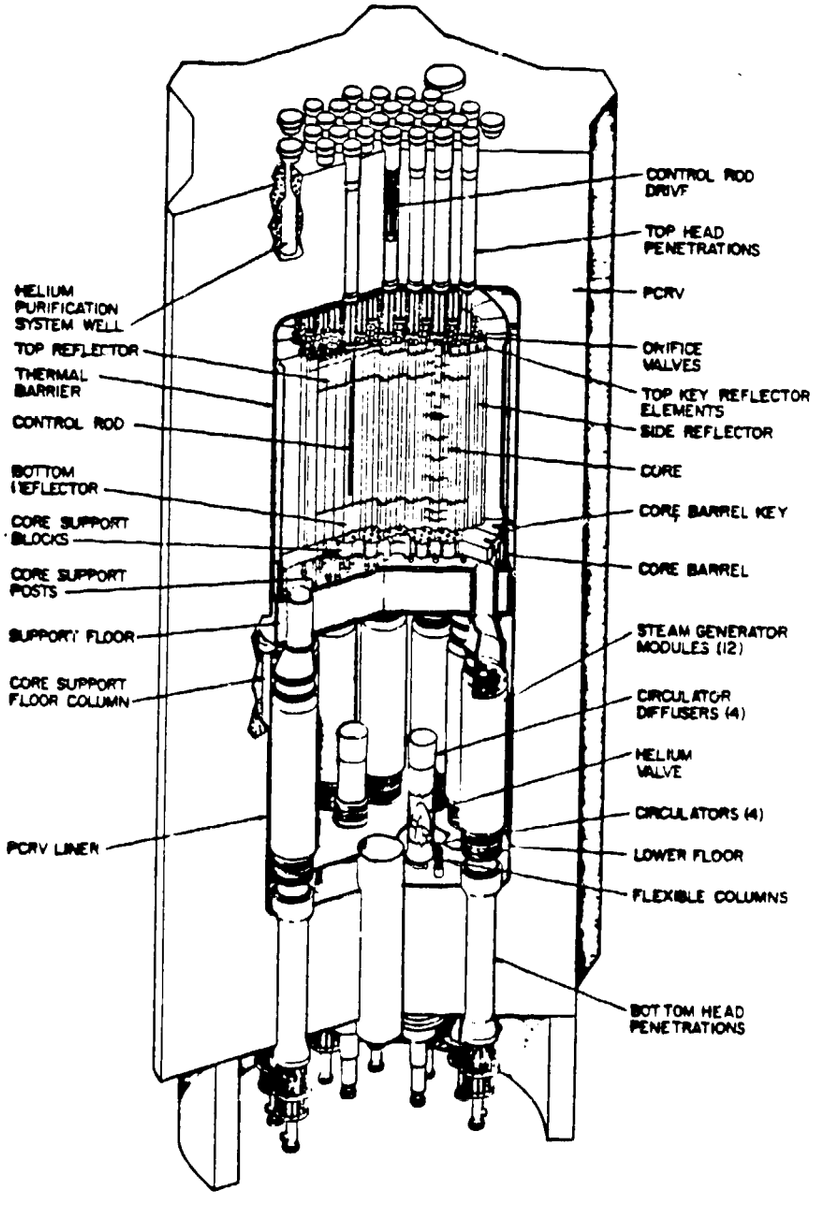

Fig. 2.
FSV reactor (from Ref. 9).

reflector material. The core assembly includes vertical columns of hexagonal fuel elements arranged on a uniform triangular pitch. The fuel elements (Fig. 3) are hexagonal right prisms. The HTGR fuel consists of thorium-uranium coated particles dispersed in a graphite matrix in the form of fuel sticks in blind holes in the elements. The CHAP-2 kinetics parameters represent beginning-of-life conditions. The orifice valves for individual refueling regions are located above the top reflector. The top-reflector elements have the same coolant hole pattern as the standard fuel elements. The permanent side reflectors have no internal coolant holes. The bottom-reflector elements have varying coolant hole patterns to collect the helium flow before it enters the region support block and the lower plenum.

During normal plant operating conditions at 100% power, helium at a temperature of 681 K and a pressure of 4.8265 MPa flows downward from the upper plenum. The net thermal power of the FSV reactor at 100% capacity is 842 MW(t). Appendix B summarizes the normal FSV operating conditions at 100% power.

4. FSV REACTOR-CORE HEAT-TRANSFER MODEL

4.1 Model Description and Assumptions

The CHAP-2 code divides the FSV active reactor core into six uniform axial sections, as shown in Fig. 4. Each axial segment is assumed to be in physical contact with its two adjacent segments. The top and bottom reflectors are assumed to be in direct contact with the upper and lower active reactor-core segments, respectively. The side reflectors that border the active reactor core and the top and bottom reflectors have the noding structure shown in Fig. 4. A helium gap is assumed to exist between the side reflectors and the core region. In addition to the axial noding, CHAP allows the user to divide further the active reactor core and the top- and bottom-reflector elements in the radial direction, creating a multichannel core. Up to six wedge-shaped regions or an individual channel for each refueling region may be selected. Mass flows, pressure drops, and heat transfer are computed separately for each radial region in each axial segment.

The reactor-core heat-transfer model uses a lumped-parameter approach by defining a symmetrical triangular unit cell based on a single average coolant channel in the standard fuel element, as seen in Fig. 5. This element (Fig. 6) is defined for each radial region in each axial core and reflector segment. This unit cell, the symmetry element, consists of 1/6 of a fuel element,

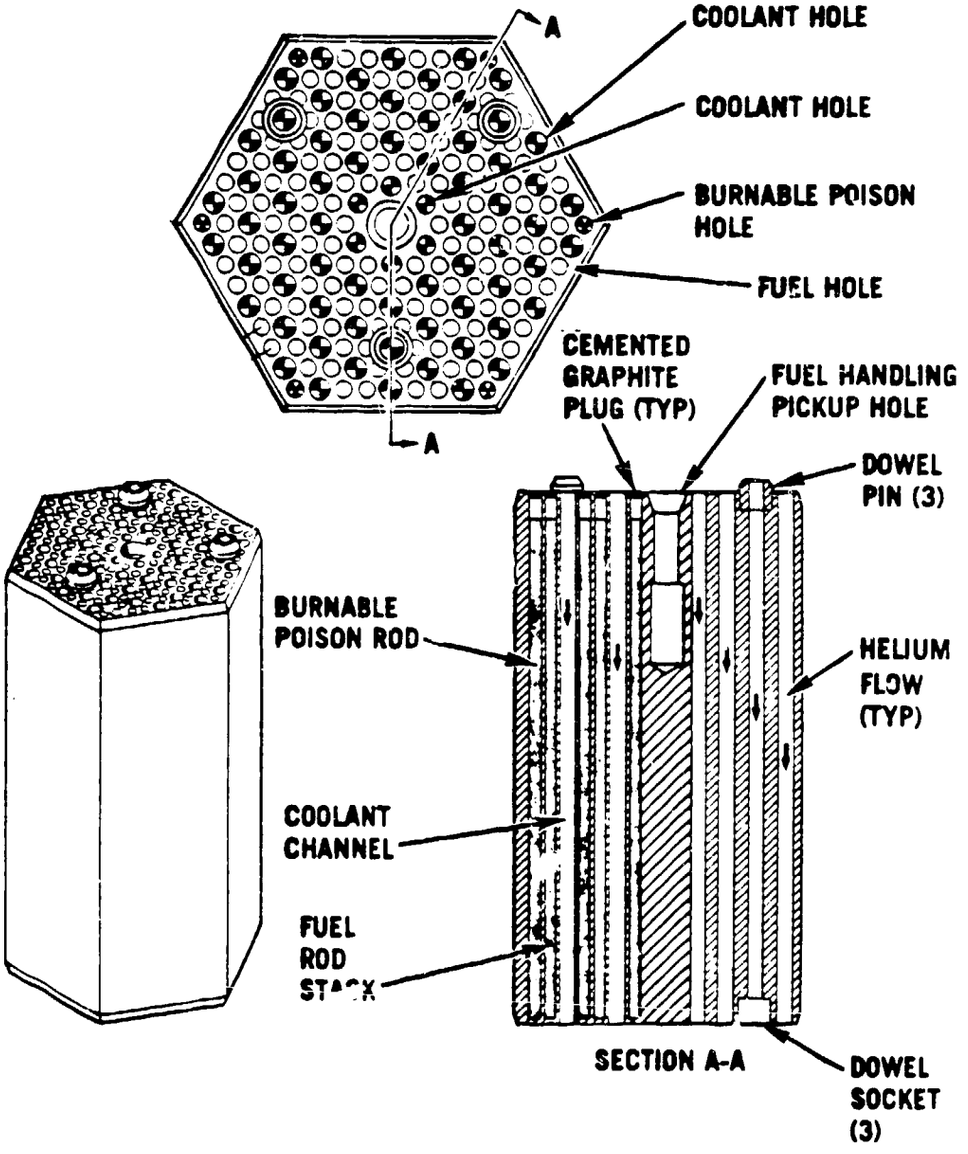

Fig. 3.
FSV core fuel element (from Ref. 9).

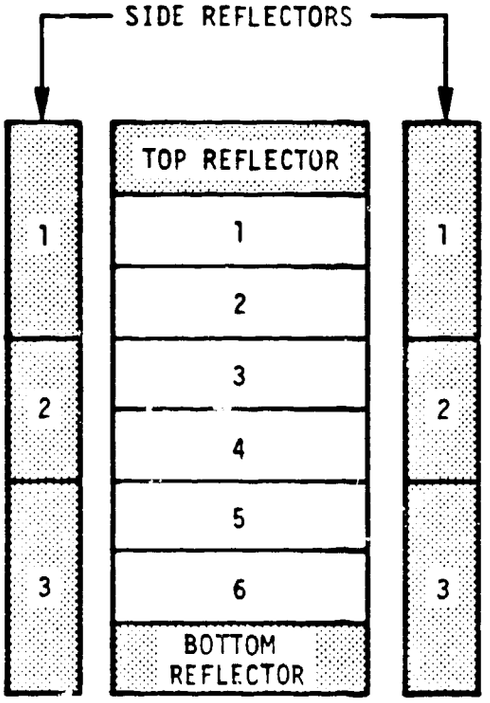

Fig. 4.
CHAP-2 axial noding of the core region.

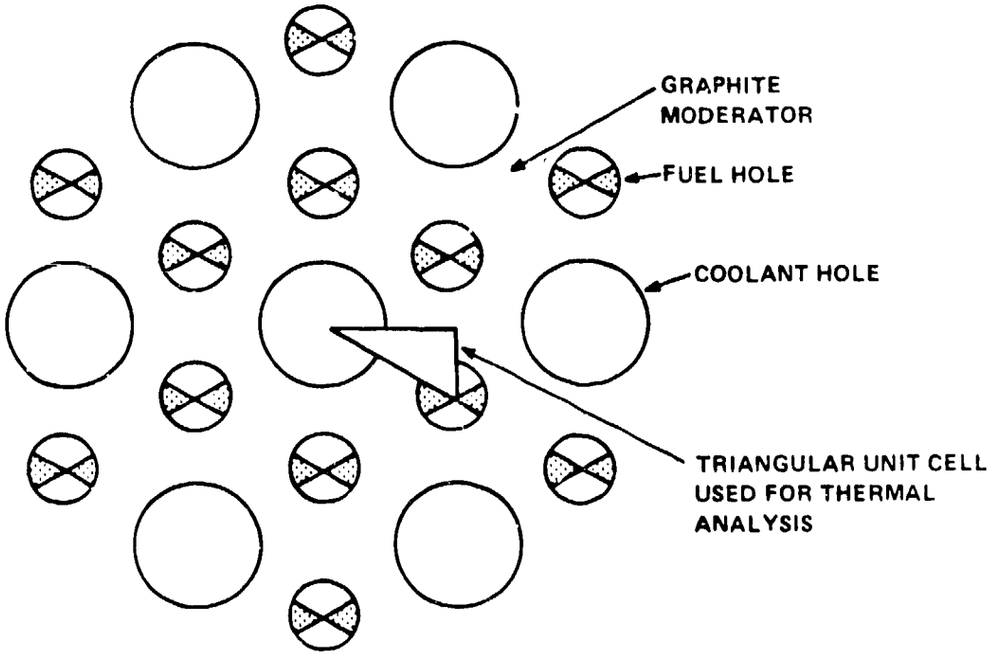

Fig. 5.
Reactor-core lumped-parameter model.

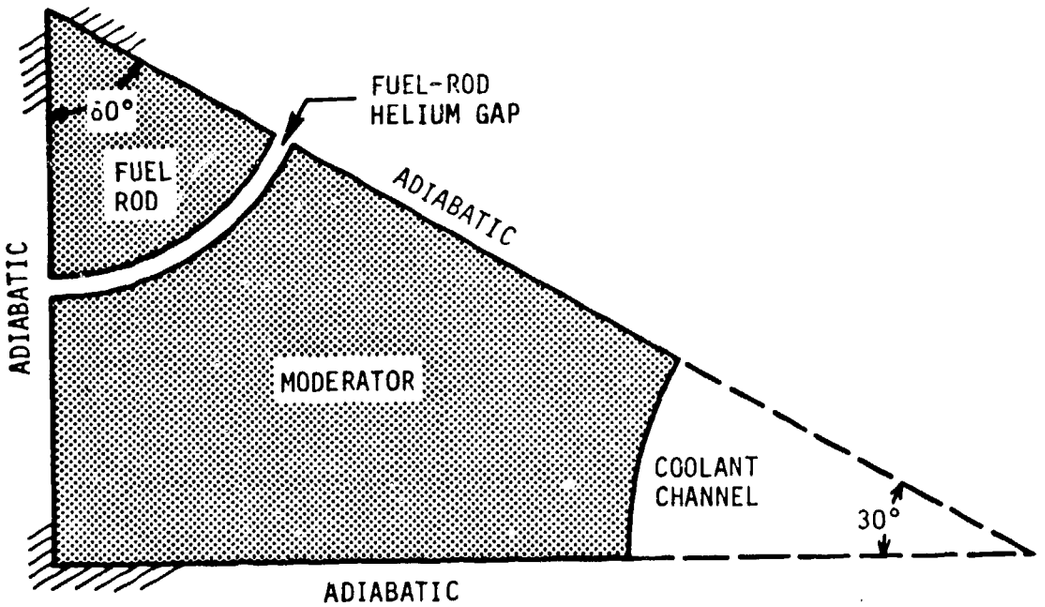

Fig. 6.
Core triangular-element geometry.

1/12 of a coolant channel, a gap between the fuel element and the moderator, and the graphite moderator material. Adiabatic boundary conditions are assumed on symmetry lines.

The code models the following heat-transfer mechanisms.

(1) Conduction heat transfer within the fuel rod.

(2) Conduction and radiation heat transfer from the fuel-rod surface to the moderator surface, across the helium gap.

(3) Conduction heat transfer within the moderator.

(4) Convection heat transfer from the moderator to the helium coolant.

(5) Conduction heat transfer between adjacent radial core sections in the same axial segment.

(6) Conduction heat transfer between adjacent axial segments, including the top and bottom reflectors.

(7) Internal heat generation caused by direct fuel fission and fission-product decay.

(8) Conduction heat transfer between each axial segment and the side reflector.

These calculations require the following assumptions.

(1) Primary-coolant thermal-inertia and mass-storage effects are neglected.

(2) Average core power from the point-reactor neutron-kinetics model is adequate.

(3) Axial and radial heat transfer occurs through the moderator material only

(4) The total coolant heat-transfer area divided by the total number of fuel rods determines the average heat-transfer area associated with a unit cell.

(5) The moderator density has been modified to account for the greater moderator mass to give the correct heat-storage effect during transients.

4.2 Steady-State Temperature Initialization of the Symmetry Element

Before CHAP-2 begins plant steady-state or transient core heat-transfer computations, a steady-state temperature gradient across the symmetry element for each active reactor-core axial section and the top and bottom reflectors must be specified. This is accomplished by using the finite-element method to compute a two-dimensional temperature map of the symmetry element. This calculation is based on the TSAAS finite-element computer program.[14] In addition to the two-dimensional temperature map, CHAP-2 initializes the helium-coolant axial inlet, outlet, and midpoint temperatures; fuel-element centerline temperature; average fuel temperature; fuel-rod surface temperature; helium-fuel gap temperature; average moderator temperature; average moderator coolant-channel surface temperature; and average convective heat-transfer coefficient for the helium coolant.

As seen in Fig. 7, the core symmetry element is subdivided into 46 quadrilateral finite elements (except for elements 1 and 2 at the fuel-rod center). Each nodal coordinate is measured relative to the 90° symmetry-triangle vertex, considered to be the origin of the r and z axes. The temperature potential or field over each of these finite elements is a function of

$$\phi_m(r,z) = [A(r,z)]_m \{\phi(t)\}_m \quad , \tag{2}$$

where $\phi_m(r,z)$ is the temperature field of element m, $[A(r,z)]_m$ is called the shape-function matrix (for a triangle), and $\{\phi(t)\}_m$ are the nodal-point temperatures. Because most of the finite elements (except for elements 1 and 2) are quadrilaterals, each element is subdivided further into four distinct triangular subelements with the common vertex at the centroid of the quadrilateral. Equation (2) then is applied separately to each subelement.

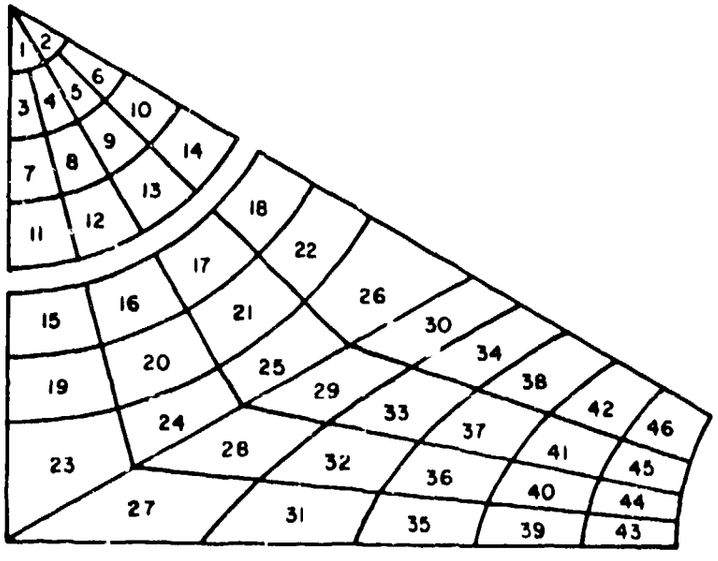

Fig. 7.
Symmetry- and finite-element noding.

Browning[14] defines the shape-function matrix $[A(r,z)]_m$,

$$[A(r,z)]^T = [D]^T\{e\} \quad , \tag{3}$$

where

$$[D] = \frac{1}{\lambda}\begin{bmatrix} 0 & 0 & 0 \\ z_j - z_k & z_k - z_i & z_i - z_j \\ r_k - r_j & r_i - r_k & r_j - r_i \end{bmatrix} ,$$

$$\lambda = r_j(z_k - z_i) + r_i(z_j - z_k) + r_k(z_i - z_j) \quad ,$$

$$\{e\}^T = (1,r,z),$$

and r_i, z_i, etc., are the coordinates of the triangular-element vertices i, j, and k.

Because the boundary conditions on the symmetry element are given, the nodal temperatures are determined by minimizing the conductivity potential V_k, defined by

$$V_k = \frac{1}{2}\{\phi\}_m^T[K]\{\phi\}_m - \{\phi\}_m^T\{Q\} \quad .$$

The global conductivity matrix [K] and the thermal flux vector {Q} for the total assembled system are given by

$$[K] = \sum_{m=1}^{M} [k]_m \quad , \quad \{Q\} = \sum_{m=1}^{M} \{\dot{q}\}_m \quad ,$$

where M is the number of finite elements in the system. The individual element conductivity is

$$[k]_m = \frac{1}{2} \int [a]_m^T [n]_m [a]_m \, dV \quad , \tag{4}$$

where $[n]_m$ is the element thermal conductivity matrix and $[a]_m$ is the shape-function gradient matrix,

$$[a]_m = \begin{bmatrix} \dfrac{\partial [A]_m}{\partial r} \\ \\ \dfrac{\partial [A]_m}{\partial z} \end{bmatrix} .$$

We assume that the symmetry element is in a steady-state condition and that thermal capacitance and inertial effects are neglected. The thermal flux vector $\{\dot{q}\}_m$ is defined,

$$\{\dot{q}\}_m = - \int_{VOL} \rho_m [A]_m^T Q^* \, dV - \int_{AREA} [A]_m^T q^* \, dS \quad , \tag{5}$$

where Q^* is the internal heat generation per unit mass and q^* is the surface flux intensity.

Because the gradient matrix $[a]_m$ does not depend on r or z, the integral in Eq. (4) may be evaluated as

$$[k]_m = [a]_m^T [n]_m [a]_m \cdot V \quad .$$

By substituting Eq. (3) into Eq. (5), we get

$$\{\dot{q}\}_m = - \rho_m [D]^T \int_{VOL} \{e\} Q^* \, dV - [D]^T \int_{AREA} \{e\} q^* \, dS \quad ,$$

The stationary conditions of the finite-element heat-conduction potential are invoked,

$$\frac{\partial V_k}{\partial \phi_i} = 0 \qquad i = 1, \ldots, N \quad ;$$

for each of the N nodal-point temperatures,

$$[K] \{\phi\}_m = \{\dot{q}\}_m \quad . \tag{6}$$

An iterative approach is used to solve Eq. (6) because the $\{\phi\}_m$ values initially are not known. An initial nodal-point temperature distribution $\{\phi_0\}_m$ is assumed for each core section to start the iteration. The iteration continues until

$$\left| 1 - \frac{\phi^{j+1}}{\phi^j} \right| < 10^{-5} \quad ,$$

where j is an iteration counter. Convergence typically occurs within four passes. This procedure is repeated for each axial segment in the model. Area-weighted average fuel and moderator temperatures are computed for each symmetry element. These temperatures are used by the CHAP-2 neutron-kinetics

model to determine the fuel and moderator feedback temperature coefficients that, in turn, are used to determine the rate of internal heat generation.

4.3 Transient Heat-Transfer Model

The basic conservation of energy equation for solid material in the symmetry element is

$$\frac{\partial(\rho Vh)}{\partial t} = \nabla \cdot (K\nabla\phi) + q''' \quad . \tag{7}$$

The local material temperature ϕ is generally a nonlinear function of total enthalpy, $H = \rho Vh$, given by

$$\phi = \phi(H)$$

In CHAP-2, Eq. (7) is replaced in CHAP-2 by equivalent lumped-node difference equations that represent average fuel and moderator temperatures in the symmetry element. These equations, written for the top-reflector element, for each axial core element of the fuel and the moderator, and for the bottom-reflector element, are:

Top Reflector

$$\frac{d(\rho Vh)}{dt} = \dot{q}_{cool} + \sum \dot{q}_{rad} + \sum \dot{q}_{ax} + \sum \dot{q}_{ref} + q''' \quad .$$

Bottom Reflector

$$\frac{d(\rho Vh)}{dt} = \dot{q}_{cool} + \sum \dot{q}_{rad} + \sum \dot{q}_{ax} + \sum \dot{q}_{ref} + q''' \quad .$$

Active-Core Section i

Moderator

$$\frac{d(\rho Vh)}{dt} = \dot{q}_{cool}^{(i)} + \sum \dot{q}_{rad}^{(i)} + \sum \dot{q}_{ax}^{(i)} + \dot{q}_{ref} + P_f^{(i)} q''' + k_{fm}(\phi_f - \phi_m) \quad .$$

Fuel Rod

$$\frac{d(\rho Vh)^{(i)}}{dt} = k_{fm}(\phi_m - \phi_f) + P_f^{(i)} q''' \quad .$$

The term q''' represents the total rate of internal energy generation from prompt fission and fission-product decay. The normalized active-core axial power distribution, assumed constant throughout any core transient, is $P_f^{(i)}$. The summation $\sum \dot{q}_{ax}$ is the conduction heat transfer between adjacent axial nodes. It consists of the net conduction energy transfer both between the upper and the lower nodes and between the sandwiched node. The top and bottom reflectors consider this energy contribution for one axial node only, because we assumed that a combined radiation and convection boundary condition exists on the plenum side. The value $\dot{q}_{ax}$ is based on an average weighted temperature ϕ_{AV} given by

$$\phi_{AV} = \frac{V_m \phi_m + V_f \phi_f}{V_m + V_f} \quad ,$$

where V_m and V_f are the moderator and fuel-element axial volumes. The heat-transfer rate $\dot{q}_{ax}$ between axial sections (i) and (i + 1) is then

$$\dot{q}_{ax} = k(\bar{\phi}) A(\phi_{AV}^{(i+1)} - \phi_{AV}^{(i)}) \quad ,$$

where A is the cross-sectional heat-transfer area and $k(\bar{\phi})$ is a thermal conductivity based on an average temperature $\bar{\phi}$,

$$\bar{\phi} = \frac{1}{2}\left[\phi_{AV}^{(i+1)} - \phi_{AV}^{(i)}\right] \quad .$$

All thermal conductivities are nonlinear functions of temperature determined by CHAP-2 through interpolation in a given data table.

The summation $\sum \dot{q}_{rad}$ is the net energy transfer between adjacent radial sections on the same axial level. For a one-channel core this component is zero. The term $\dot{q}_{rad}$ is computed between adjacent core regions (i) and (j) for each axial node by

$$q^{(i)} = A_s f_c F_{ij} k(\bar{\phi})\left[\phi_m^{(i)} - \phi_m{}^{(j)}\right] \quad ,$$

where A_s is a design data parameter ensuring the proper heat-transfer rate at design conditions; f_c, the ratio of axial segment length to total core height; F_{ij}, the fractional contact area between regions (i) and (j), and $k(\bar{\phi})$, the equivalent radial conductivity based on an average temperature $\bar{\phi}$ given by

$$\bar{\phi} = \frac{1}{2}\,\phi_m^{(i)} + \phi_m^{(j)} \quad .$$

The term $\dot{q}_{r,f}$, the heat-transfer rate between the central core region and the side reflector, is given by

$$q_{r,f}^{(i)} = \sum_{\ell=1}^{m} \left\{A_s F_{ij} f_r^{(i)} k(\bar{\phi}) \phi_c^{(j)} - \phi_{SR}^{(i)}\right\} \quad ,$$

where i is the side-reflector index (1, 2, or 3); m, the number of core regions (j) adjacent to side reflector (i); $f_r^{(i)}$, the ratio of the height of the side-reflector axial segment (i) to the total side-reflector height; $\phi_{SR}^{(i)}$, the average temperature of side reflector (i); and $\phi_c^{(j)}$, an average core axial temperature is given by

$$\phi_c^{(j)} = \sum_{k=J1}^{J2} \frac{f_c^{(k)}}{f_r^{(j)}} \cdot \phi_m^{(k)} \quad ,$$

where J1 and J2 are indices of core axial nodes corresponding to side-reflector axial segment (i) and $k(\bar{\phi})$ is the equivalent conductivity based on an average temperature $\bar{\phi}$ given by

$$\bar{\phi} = \frac{i}{2} [\phi_c^{(j)} + \phi_{SR}^{(i)}] \quad .$$

Conduction and radiation heat transfer from the fuel rod to the moderator is accounted for in the term,

$$k_{fm}(\phi_f - \phi_m) \quad ,$$

where the overall conductivity k_{fm} is defined to be

$$k_{fm} = \frac{1}{\frac{1}{k_m} + \frac{1}{k_f} + \frac{1}{k_g}} \quad .$$

In this expression k_m is the average moderator thermal conductivity; k_f, the average fuel-rod conductivity; and k_g, the average helium-gas conductivity. The term k_g, a composite of conduction and radiation effects, is determined by

$$k_g = A\left[\frac{k(\bar{\phi})}{\Delta g} + 4\sigma\varepsilon(\bar{\phi})^3\right] \quad ,$$

where Δg is the helium-gap width; A, the mean gap heat-transfer area; σ, the Stefan-Boltzmann constant; ε, the mean gap emissivity; and $\bar{\phi} = 1/2(\phi_f + \phi_m)$, the average helium-gap temperature.

The final heat-transfer term $\dot{q}_{cool}$ represents the average energy gain of the helium coolant through one axial core node or the top or bottom reflector. A quasi-static energy balance on the coolant-channel surface gives

$$Wc_p \frac{d\bar{T}(x)}{dx} = \frac{\bar{U}\bar{A}}{L}\phi(x) - \bar{T}(x) + \frac{\dot{q}_e}{L} \quad ,$$

where $\dot{q}_e$ is an additional external heat source and the bars indicate quantities averaged over the channel length L. For a wall temperature distribution given by

$$\phi(x) = \bar{\phi} + \Delta\phi\left(\frac{x}{L} - \frac{1}{2}\right) \quad ,$$

an analytical solution for T(x) can be obtained such that

$$T(x) = T_0 \exp(-\beta x) + \left[\frac{1 - \exp(-\beta x)}{\beta Wc_p L}\right]\left\{UA\left(\bar{\phi} - \frac{\Delta\phi}{\beta L} - \frac{\Delta\phi}{2}\right) + \dot{q}_e\right\} + \frac{x}{L}\Delta\phi \quad , \qquad (8)$$

where

$$\beta = \frac{\overline{UA}}{\dot{W}c_p L} \quad .$$

The outlet temperature is obtained by evaluating Eq. (8) at x = L. The average fluid temperature $\overline{T}$ is obtained from

$$\overline{T} = \frac{1}{L}\int_{x=0}^{x=L} T(x)\,dx = T_0[1 - \exp(-\beta L)$$

$$- \left[\frac{1 - \exp(-\beta L) - \beta L}{\beta L \overline{UA}}\right]\left[\overline{UA}\left(\overline{\phi} - \frac{\Delta\phi}{\beta L} - \frac{\Delta\phi}{2}\right) + \dot{q}_e\right] + \frac{\Delta\phi}{2} \quad .$$

The equations above also are valid for $\Delta\phi = 0$, $\dot{q}_e = 0$, or both equal to zero. The heat-transfer rate $\dot{q}_{cool}$ from the fluid to surface (i) can be calculated from

$$\dot{q}_{cool} = \overline{UA}(\overline{T} - \overline{\phi}) \quad . \tag{9}$$

The laminar ($h_{c\ell}$), turbulent (h_{ct}), and transition (h_{ci}) convective heat-transfer coefficients are found by

$h_{c\ell} = 3.66\ k/D$ for $Re < 2300$,

$h_{ct} = 0.023\ k/D\ Re^{0.8}Pr^{0.4}$ for $Re > 4000$,

or

$h_{ci} = h_{c\ell} + (Re - 2300)(h_{ct} - h_{c\ell})/1700$ for $2300 < Re < 4000$.

The fluid properties used in this calculation are based on the film temperature (the arithmetic average of $\overline{T}$ and $\overline{\phi}$) so CHAP-2 calculates a surface temperature from

$$\overline{\phi}' = \overline{T} - \frac{\dot{q}_{cool}}{h_c A} \quad .$$

The heat-transfer coefficients are a function of the film temperature as well as the mass flow and the geometry, so the algorithm iterates on h_c until the relative change in that sum between iterations is less than a specified convergence criterion.

5. CONTROL-ROD WITHDRAWAL ACCIDENT ANALYSIS

5.1 Problem Definition and Assumptions

Reference 13 states that the greatest reactivity insertion and the largest credible reactivity insertion rate in the FSV reactor result from the accidental withdrawal of control poison. In this problem we assume that the FSV reactor is at the steady-state conditions delineated in Appendix B and that the control-rod pair is withdrawn from a 25% insertion position at an average rate of 6.25×10^{-3} %/s. Because the FSV control rod has a total worth of 0.015 Δk, this accident represents a reactivity addition of 0.00375 Δk. Also, because the rod worth as a function of degree of withdrawal is nearly linear,[13] the average reactivity addition rate is 0.000094 Δk/s.

In this paper we examine only the core transient heat transfer and exclude the secondary-side components and the controls that govern them. However, the protective control system remains operative for this problem, thereby, providing scram action when unsafe conditions, as defined in the FSV FSAR,[13] occur. Computational time is minimized by using the one-channel core model with one set of differential equations per axial section. Helium flow through the core during the rod withdrawal remains constant, but is ramped down at a rate of 0.00167 %/s when the reactor scrams. This rate roughly corresponds to the feedwater rampdown during a reactor scram and is used because the feedpump and helium-circulator models are not included in this problem. The CHAP-2 modules used are BOUNDS, UPPLEN, CORE, KINET, REFL, CTLROD, and LOWPLN (see Appendix A for definitions).

5.2 Summary of Results

The sequence of events for this analysis of the control-rod withdrawal accident is as follows. At 0.0 s, the control rod begins to withdraw from the core, causing the core thermal power to increase at a linear rate of 18.54 MW/s (Fig. 8). The fuel rods, moderator, and helium coolant in all axial segments experience a slow temperature rise. The scram set point of 140% prompt neutron power (corresponding to a total core power of 1145 MW) is reached at 16.345 s, initiating a reactor scram. At this point the control rod has withdrawn to the 18% insertion position, representing a total core reactivity gain of 0.00105 Δk. A maximum fuel-rod centerline temperature of 1173.8 K is reached at the fourth axial core section, up 11 K from the initial temperature (Fig. 9). The scram causes all rods, including the control rod, to insert at 6.22×10^{-3} %/s and the coolant flow to ramp down 0.00167 %/s. This action rapidly decreases the prompt neutron power, terminating the withdrawal accident. Although the fuel-rod temperatures decrease immediately when the reactor scrams, both the moderator and helium-coolant temperatures continue to increase for 6 s. The maximum moderator temperature occurs at the sixth axial section at 1100.3 K, up 9 K from the initial temperature (Fig. 10). The helium coolant experiences the greatest temperature rise of 11 K at the fourth and fifth axial core section inlets (Fig. 11). This temperature lag is due to the thermal inertia of the graphite. After this slight additional temperature increase, both the moderator and helium coolant experience a rapid temperature decrease. As seen in Fig. 8, the prompt neutron power decline occurs rapidly after the onset of the reactor scram, averaging 40.5 MW/s in the 24 s after the scram. The fission-product decay-power decline is less severe and at 150 s represents 98.3% of the total core power. Both fission-product decay and prompt neutron power continue to decrease slowly after 150 s until reactor shutdown conditions occur.

6. SUMMARY

Los Alamos developed the CHAP-2 code to examine the total plant response of a gas-cooled reactor plant to a variety of postulated accidents and operating transients. The CHAP-2 reactor-core heat-transfer model has been discussed and a control-rod withdrawal accident simulated to display the capabilities of the code.. The heat-transfer model initializes the fuel-rod moderator, and the helium-coolant temperatures and heat-transfer coefficients by using the finite-element method. The transient behavior of the core is modeled by a set of dynamic equations written for the fuel rod and the moderator in each axial core section and for the top and bottom reflector.

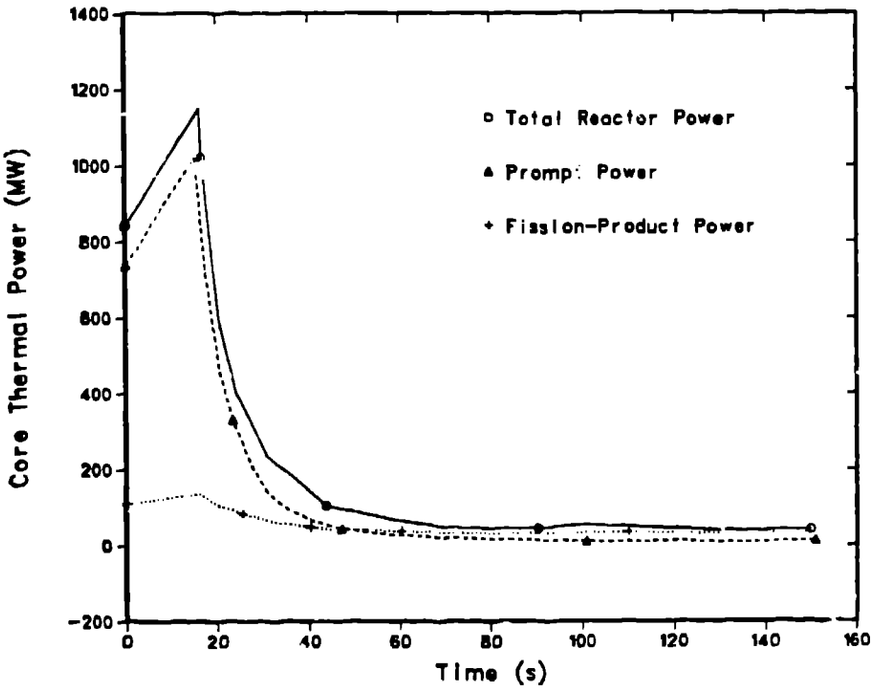

Fig. 8.
Core thermal power.

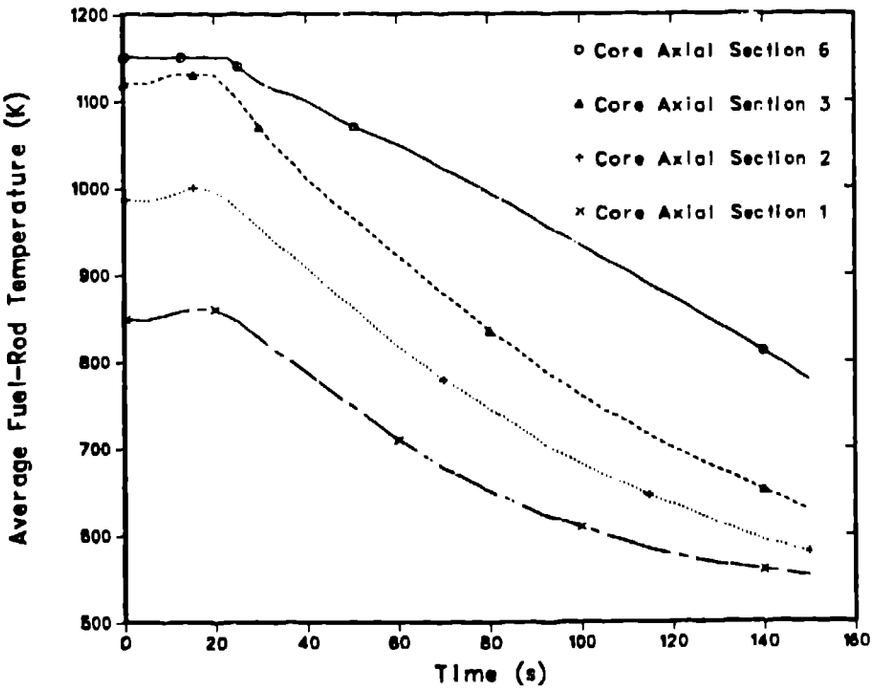

Fig. 9.
Fuel-rod temperatures at axial sections 1, 2, 3, and 6.

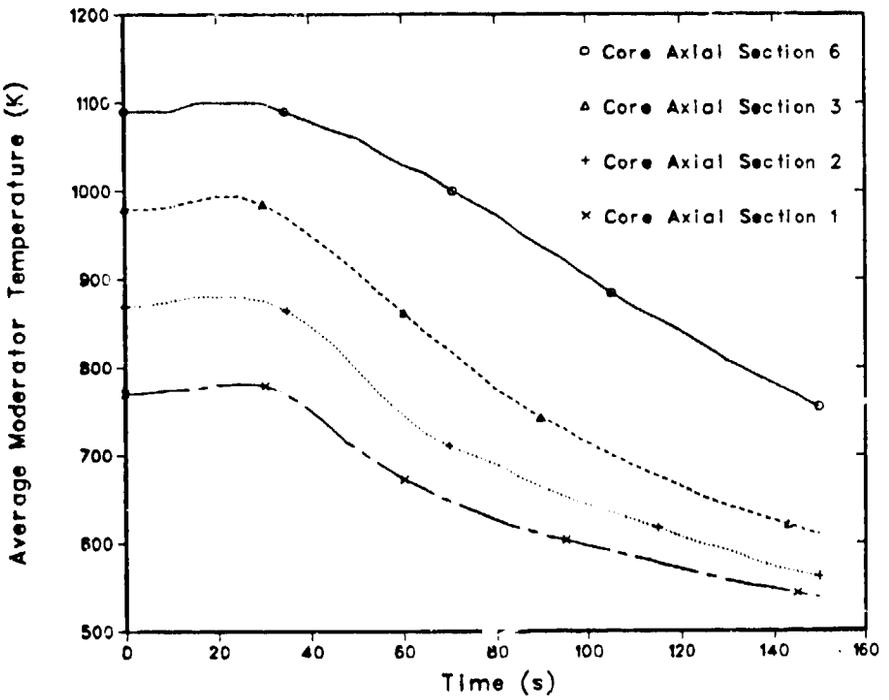

Fig. 10.
Moderator temperatures at axial section 1, 2, 3, and 6.

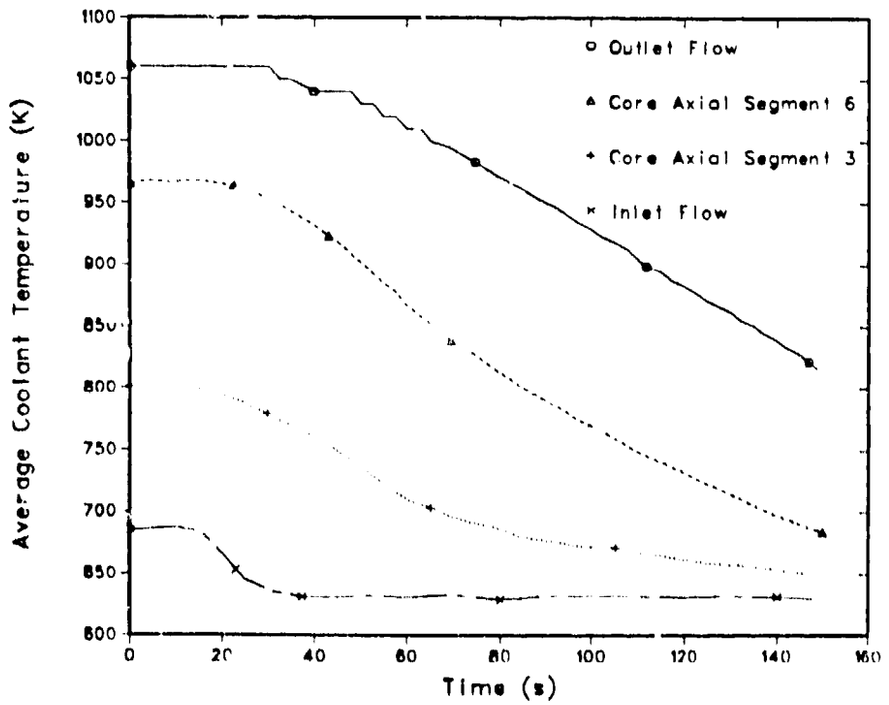

Fig. 11.
Coolant temperatures at the core inlet, axial section 3, axial section 6, and the core outlet.

APPENDIX A

CHAP-2 MODULES

Module	Description
AUXCCS	Models the core auxiliary-cooling-system dynamics for both standby and operational conditions for the large HTGR plant.
BOUNDS	Provides initial and time-dependent boundary conditions for all modules.
CIRDUC	Models the duct thermal hydraulics between the helium-circulator exit and the upper plenum for the large HTGR plant.
CNTMNT	Models the containment-building dynamics during prestressed-concrete reactor-vessel depressurization accidents.
CORE	Models the active reactor core and the top and bottom reflectors.
CTLFED	Models the proportional integral derivative (PID) controllers in the feedwater system.
CTLHEC	Models the helium-circulator speed and pressure PID controllers.
CTLHPT	Models the PID controller in the high-pressure turbine/bypass system.
CTLLPT	Models the PID controllers in the low-pressure turbine/bypass system.
CTLROD	Models the PID controller and the dynamics of the control rod.
FEDWTR	Models the feedwater system including the feedwater heaters, steam extractors, boiler feedpumps and turbine, and condensate pumps.
FSVRHT	Models the reheater for the FSV plant
FSVSTG	Models the steam generator for the FSV plant.
HAZARD	Provides a radionuclide relative hazard index for normal and transient plant operation.
HECIRC	Models the dynamics of the helium circulator.
HPTBYP	Models the high-pressure turbine (HPT) and the bypass system including the HPT desuperheater and the flash tank.
KINET	Models the point-reactor neutron kinetics and the decay-power dynamics.
LOWPLN	Models the core lower-plenum thermal hydraulics.
LPTBYP	Models the low- and intermediate-pressure turbines and the bypass system including the low-pressure turbine desuperheater.
REFL	Models the side reflector and the peripheral regions.
REHTR	Models the reheater for the large HTGR plant.
RHTDUC	Models the duct between the lower plenum and the reheater.
STMGEN	Models the steam generator for the large HTGR plant.
UPPLEN	Models the core upper-plenum thermal hydraulics.

APPENDIX B

SUMMARY OF THE FSV REACTOR OPERATING CONDITIONS AT 100% POWER

Net thermal power	842 MW(t)
Net electrical power	330 MW(t)
Plant efficiency	39.1%
Design-plant capacity factor	85%
Average core power density	6.3 kW/ℓ
Percentage of prompt fission power	87.2%
Percentage of fission-product decay power	12.8%
Primary-coolant flow rate	440.124 kg/s
Percentage of flow through the side-reflector region	3.5%
Total primary-coolant inventory	3.356618 Mg
Core inlet temperature	681 K
Core inlet pressure	4.8265 MPa
Core Pressure drop	69.5 kPa
Core outlet temperature	1049 K
Core outlet pressure	4.757 MPa
Maximum fuel temperature	1573 K
Short-term peak fuel temperature	1773 K
Maximum moderator temperature	1450 K
Maximum surface heat flux at coolant-channel surface	10.55 $\frac{cal}{s \cdot cm^2}$
Average flux at coolant-channel surface	3.39 $\frac{cal}{s \cdot cm^2}$
Maximum primary-coolant Reynolds number	6.7×10^4
Average primary-coolant Reynolds number	2.5×10^4
Maximum surface heat-transfer coefficient	0.0542 $\frac{cal}{s \cdot cm^2 \cdot {}^oC}$
Average surface heat-transfer coefficient	0.0312 $\frac{cal}{s \cdot cm^2 \cdot {}^oC}$

REFERENCES

1. M. H. Merrill, "BLOOST-7, A Reactor Kinetics-Heat Transfer Program for the UNIVAC-1108," General Atomic Company report GA-9832 (January 1970).

2. H. W. Chi and G. J. Malek, "Description of the Reactor Emergency Cooling Analysis Code, RECA," General Atomic Company report GA-10273 (August 1970).

3. K. E. Scwartztrauber and F. A. Silady, "CORCON: A Program for Analysis of HTGR Core Heatup Transients," General Atomic Company report GA-A12868/GA-LTR-13 (July 1974).

4. A. Bardia and R. C. Potter, "TAP: A Program for Analysis of HTGR Nuclear Steam Supply System Performance Transients," General Atomic Company report GA-A13248/GA-LTR-21 (January 1976).

5. R. K. Deremer and T. Shih, "RATSAM: A Computer Code to Analyze the Transient Behavior of the HTGR Primary Coolant System During Accidents," General Atomic Company report GA-A13705 (May 1977).

6. J. F. Peterson, "RECA3: A Computer Code for Thermal Analysis of HTGR Emergency Cooling Transients," General Atomic Company report GA-A14520/GA-LTR-22 (August 1977).

7. S. J. Ball, "ORECA-I: A Digital Computer Code for Simulating the Dynamics of HTGR Cores for Emergency Cooling Analyses," Oak Ridge National Laboratory report ORNL/TM-5159 (April 1976).

8. J. C. Cleveland, "CORTAP: A Coupled Neutron Kinetics-Heat Transfer Digital Computer Program for the Dynamic Simulation of the High-Temperature Gas-Cooled Reactor Core," Oak Ridge National Laboratory report ORNL/NUREG/TM-39 (January 1977).

9. J. C. Cleveland, R. A. Hedrick, S. J. Ball, and J. G. Delene, "ORTAP: A Nuclear Steam Supply System Simulation for the Dynamic Analysis of High-Temperature Gas-Cooled Reactor Transients," Oak Ridge National Laboratory report ORNL/NUREG/TM-78 (September 1977).

10. J. S. Gilbert, P. A. Secker, Jr., J. C. Vigil, M. J. Wecksong, G. J. E. Willcutt, Jr., "User's Manual for the Composite HTGR Analysis Program (CHAP-1)," Los Alamos Scientific Laboratory report LA-NUREG-6576-M (March 1977).

11. J. F. Kotas, K. R. Stroh, and J. Stanford, "CHAP-2, An Advanced Best-Estimate Computer Program for High-Temperature Gas-Cooled Reactor Accident Analysis," Los Alamos National Laboratory report (to be published).

12. K. R. Stroh, P. A. Secker, R. B. Lazarus, and P. L. Rivera, "User's Manual for LASAN, A General Systems Analysis Code for Large Scale Model Simulations," Los Alamos National Laboratory report (to be published).

13. Public Service Company of Colorado, "Fort St. Vrain Nuclear Generating Station: Final Safety Analysis Report," Atomic Energy Commission docket number 50-267 (1967).

14. R. V. Browning, D. G. Miller, and C. A. Anderson, "TSAAS: Finite Element Thermal and Stress Analysis of Axisymmetric Solids with Orthotropic Temperature-Dependent Material Properties," Los Alamos scientific Laboratory report LA-5599-MS (May 1974).